



LAWRENCE
LIVERMORE
NATIONAL
LABORATORY

LLNL-JRNL-652735

Enabling membrane protein structure and dynamics with x-ray free electron lasers

G. K. Feld, B. W. Segelke, M. Frank

April 7, 2014

Current Opinion in Structural Biology

Disclaimer

This document was prepared as an account of work sponsored by an agency of the United States government. Neither the United States government nor Lawrence Livermore National Security, LLC, nor any of their employees makes any warranty, expressed or implied, or assumes any legal liability or responsibility for the accuracy, completeness, or usefulness of any information, apparatus, product, or process disclosed, or represents that its use would not infringe privately owned rights. Reference herein to any specific commercial product, process, or service by trade name, trademark, manufacturer, or otherwise does not necessarily constitute or imply its endorsement, recommendation, or favoring by the United States government or Lawrence Livermore National Security, LLC. The views and opinions of authors expressed herein do not necessarily state or reflect those of the United States government or Lawrence Livermore National Security, LLC, and shall not be used for advertising or product endorsement purposes.

**Enabling membrane protein structure and dynamics with X-ray free electron
lasers**

Geoffrey K. Feld,^a Brent W. Segelke,^a Matthias Frank^{b*}

^aBiosciences and Biotechnology and ^bPhysics Divisions, Physical and Life Sciences
Directorate, Lawrence Livermore National Laboratory, Livermore, CA, U.S.A.

Running title: bioXFEL review

***Address correspondence to:** Matthias Frank, Ph.D., Lawrence Livermore National
Laboratory, 7000 East Ave, L211, Livermore, CA 94550. Phone: 925-423-5068 Email:
frank1@llnl.gov (M.F.)

Introduction

In 2009, the Linac Coherent Light Source (LCLS) at the Stanford Linear Accelerator Center (SLAC) was commissioned, delivering world's first X-ray free electron laser (XFEL) pulses. Each pulse delivers $\sim 10^{12}$ photons within a few tens of femtoseconds at 120 Hz, realizing the “diffract-before-destroy” principle that was first proposed using computer simulations only nine years prior (1). Since then, a second hard XFEL (SACLA) turned on in Japan, and the world awaits two new XFEL instruments in Germany and Switzerland to be completed in 2016 (2). While this photon flux is still short of the theoretical threshold necessary for single molecule atomic resolution imaging, it has opened the door to X-ray structure determination of micro- and nano-sized crystals at room temperature (3) to high resolution (4), low-resolution imaging of single virus particles (5) and cells (6), as well as the quantifying time-resolved structural changes from biological samples that either require faster temporal resolution or have unit cells too large for Laue diffraction studies at synchrotron radiation sources (7). The study of membrane proteins with XFELs has garnered expectedly prodigious effort and interest from the structural biology community, as these molecules are rich with structural information germane to medicine and energy; yet they notoriously resist crystallization and are radiation sensitive.

Most of the recent XFEL biological imaging experiments have used the Coherent X-ray Imaging (CXI) endstation at LCLS (8), where a typical setup includes an XFEL source, a sample environment where specimens are delivered to the XFEL beam, and one or two pixel array X-ray detectors (for a review of initial biological XFEL results and instrumentation, see refs. (9-11)). The sample environment allows for additional instruments to be included, permitting simultaneous data collection of orthogonal measurements. Because an unattenuated XFEL pulse completely ionizes a biological sample, each successful shot results in one diffraction pattern being collected from one ultimately destroyed specimen. This necessitates serial replenishment of the sample and the patterns to be read off the detector after each pulse. In the case of serial femtosecond crystallography (SFX), the near instantaneous interaction of crystal with XFEL

beam has two important consequences. On one hand, Bragg diffraction is essentially gated by radiation damage inherent to the pulse length, meaning the loss of order incurred during longer pulses does not contribute to the recorded reflections (12,13). On the other hand, the crystal does not rotate during the pulse duration, resulting in “still” diffraction patterns that lack partially information. As a result, a number of technical challenges related to sample delivery, detector technology, data acquisition and analysis must be overcome for successful execution of experiments. In this review, we report on the recent steps taken towards ameliorating some of these challenges and the exciting investigations into membrane proteins that depended on these advancements. We further speculate on future advancements, experiments, and limitations. Ultimately, the hope is the enormous financial and intellectual investment in X-ray laser facilities will result in our better understanding of biological processes.

***In vivo* crystallization**

It has long been known that protein crystallization occurs both naturally *in vivo*; however, only recently with the advent of SFX could these small crystals be exploited for structural studies (14). Cathepsin, a glycosylated cysteine protease from *Trypanosoma brucei* (TbCatB), the causative agent of African trypanosomiasis, represents a potential target for countermeasures against the protozoan pathogen; however, structural analysis of the protein has only yielded models of the mature enzyme in the absence of glycosylation. When the protein is expressed as a chimera with a virus polyhedron promoter in Sf9 insect cells, it forms microcrystals *in vivo*. Using SFX, the fully glycosylated protease structure was determined to 2.X-Å resolution, providing an important template for rational drug design and potential treatments against the neglected African sleeping sickness (15). Further investigations into *in vivo* crystallization inside baculovirus-transfected insect cells that can be exploited by SFX may open an entirely new route to structural biology pipelines of difficult targets, including membrane proteins.

Sample delivery strategies

A recurring challenge in SFX is the amount of sample required for structure solution. An obvious point in the experiment for improvement is increasing the number of crystal “hits” relative to empty shots where the XFEL beam did not intercept a crystal. The workhorse of SFX experiments to date has been the gas dynamic virtual nozzle (GDVN), which nominally delivers fully hydrated crystals to the XFEL beam at $\geq 10 \mu\text{L min}^{-1}$ flow rates (16). While successful, reducing the velocity of the liquid column, and thus increasing successful crystal hits, has been a primary focus. A microflow electrospin platform operating at $\sim 3 \mu\text{L min}^{-1}$ enabled a number of SFX experiments (17-19) by extending the length of the microjet in an applied electric field. A proof-of-concept SFX interrogation of 30S ribosomal subunits was recently demonstrated (19), opening the door to structural studies involving complex translational machinery that may resist macro-crystallization, as well as time-resolved X-ray studies of molecules with unit cells too large to image with Laue diffraction at synchrotrons (7). Further development of the electrospinning system resulted in a stable nanoflow jet with flow rates $\leq 0.14 \leq 3 \mu\text{L min}^{-1}$ (20). However, this lower flow regime requires the sample solution to contain viscous additives such as glycerol; sample stability may therefore be crystal dependent.

Injection of viscous lipidic cubic phase (LCP) represents another opportunity to reduce the column velocity, as well as provide a membrane mimetic environment that has proven successful for growing well-ordered crystals of membrane proteins, especially G protein-coupled receptors (GPCRs) (21). Recent development of a novel LCP injector facilitated the SFX structure solution at LCLS of the human smoothened Frizzled-class receptor (SMO) in complex with the naturally-occurring potential anti-tumor antagonist cyclopamine (22) and the human 5-HT_{2B} receptor (23). Interestingly, the authors report that the SMO-cyclopamine complex also formed larger crystals suitable for synchrotron data collection; however, these crystals diffracted poorly. This suggests the smaller microcrystals are better ordered, possibly due to fewer chances

for imperfections to develop during crystal formation. The ingenious hydraulic pump-style design of the injector permits 1-300 nL min⁻¹ flow rates of gel-like LCP that can be tuned to the XFEL repetition rate by adjusting the hydraulic fluid pressure; thus minimizing sample waste. In these studies, full data sets could be collected from ~0.5 mg total protein, a 20-30-fold improvement over samples injected via the GVDN. A key obstacle surmounted in the LCP jet injector centered around the monoolein lipid (MAG 9.9*) commonly used for *in meso* crystallization. This lipid undergoes a phase change to a lamellar crystalline (L_c) phase just under room temperature, which occurred readily in the vacuum sample environment, resulting in strong background diffraction rings. Addition of shorter chain lipids, including monopalmitolein and a novel 7.9 MAG, post crystallization suppressed the formation of the L_c phase, resulting in much cleaner backgrounds. The authors report that this post-crystallization addition of lipids does not dissolve or damage the crystals used in the study; it remains to be seen whether this strategy is widely applicable to other membrane proteins.

As opposed to injection, an alternative sample delivery approach involves mounting specimens on a fixed “target” and replenishing the beam with fresh samples via a translating stage. In this manner, a 100% hit rate may be theoretically achieved, assuming a monolayer of crystals or specimens. The main experimental considerations necessary for such an approach include using very thin X-ray transmissible materials as the target substrate and protecting hydration-sensitive samples from vacuum-induced evaporation. Researchers at SACLAC constructed a micro-liquid enclosure array from a sandwich of thin (10s of nm) silicon nitride wafers to perform coherent diffractive imaging of single live *Microbacterium lacticum* cells (6). A proof-of-principle fixed-target chip was developed and tested at a synchrotron that attempted to randomize the orientations of crystals by surface heterogeneity, which may help in further reducing the number of shots required for convergence (24). Both of these wafers required individual “windows” whereas one XFEL pulse was shot at one window in burst mode; new

methods must be developed to take full advantage of the high repetition rate of the LCLS (120 Hz) and future European and Swiss FELs (10 kHz). [More...table](#)

- Soltis pubs? → submitted acoustic delivery manuscript; gonio+grid manuscript in preparation (soon)

Data analysis and phasing methods

An enormous amount of data is produced quickly by SFX; detector readout speed and dataset size are measured in seconds and gigabytes at synchrotrons and milliseconds and terabytes at XFELs, respectively. The nature of the experiment gives rise to a host of variables that complicates diffraction image processing, including (but not limited to) nonzero pulse-to-pulse bandwidth of XFEL “jitter”, random orientations of variably sized crystals, the recording of only partial reflections from a nonrotating crystal, and the metrology of aligning the individual components of the complex CSPAD detector.. As is the case with conventional X-ray crystallography, expert groups worldwide have implemented user-friendly software packages for efficient data reduction and processing of the unique image files into scaled data sets, which then can be interpolated into existing macromolecular structure software pipelines. The recently developed *Cheetah* data reduction package (25) includes a graphic user interface (GUI) allowing users to inspect frames almost in real-time, and through publically available scripts seamlessly integrate with the existing *CrystFEL* platform (26) for Bragg reflection indexing using a Monte Carlo approach (27). In a simulation study, White *et al* showed it is theoretically possible to reduce the number of partially recorded reflection observations necessary for convergence during Monte Carlo integration if the beam divergence and/or bandwidth are increased (25). Conversely, it is unclear to what extent the myriad of other data collection factors contributes to convergence. A Python-based platform for almost real-time Bragg reflection analysis and data reduction has recently become available that adds to and exploits existing online capabilities of the computational crystallography toolbox, giving rise to cctbx.xfel (28). This package makes light of

the importance of metrology to efficient data collection, requiring subpixel precision. Combining this with multicrystal deconvolution strategies from synchrotron work enables cctbx.xfel to reach integration convergence using fewer crystal hits than previous SFX results (29). Thus, XFEL users can leverage multiple software tools for interpreting and processing diffraction patterns that are inherently different from conventional X-ray sources.

Until recently, complete SFX datasets could only be phased using molecular replacement, and questions remained as to the feasibility of collecting anomalous data with FEL radiation. For instance, due to ambiguities in indexing SFX data for polar point groups, anomalous phasing of structures that crystallize in these symmetries might prove to be difficult (see ref (25)). For these reasons, tetragonal ($P4_32_12$) lysozyme was selected for proof-of-principle phasing studies. During the commissioning of the multipurpose spectroscopy/imaging apparatus at SPRING-8, a highly-redundant (≥ 7500 partial reflection observations on average) dataset of HEW lysozyme was collected with 7.3 keV X-rays to 3.2-Å resolution, and anomalous differences for 7 of the 10 sulfur-containing residues were identified, as well as surface densities likely corresponding to chloride ions (30). While the structure could not be determined directly from the S-SAD data, the study did demonstrate that the Monte Carlo integration method for SFX, combined with conventional crystallographic software analysis could reveal even the minute anomalous differences associated with endogenous sulfur. Another highly redundant dataset complete to 2.1-Å resolution using 8.5 keV X-rays from LCLS resulted in the structure of HEW lysozyme to be determined exclusively by gadolinium-SAD *de novo* phasing (31). This represents an important milestone for SFX to determine structures of proteins without prior phase information using conventional heavy-atom derivatives, and paves the way for completely new structures to be determined using XFELs.

SFX of membrane proteins

Development of the LCP injector represents a critical breakthrough in the structural analysis of membrane proteins by SFX at room temperature. The structure determination of soluble proteins at near-physiological temperatures has recently garnered interest, as cryo cooling may induce the over-packing of side chains whose alternative conformers may otherwise be functionally relevant (32,33). Weierstall *et al* report on the successful room-temperature injection of and diffraction from a number of different membrane proteins in LCP (22), including diacylglycerol kinase (DgkA) and the human G protein-coupled β_2 A, A_{2AA}, SMO, glucagon, and serotonin 5-HT_{2B} receptors (23). To date, full SFX datasets suitable for structure solution were collected for DgkA, SMO in complex with cyclopamine, and 5-HT_{2B}. The cryocooled structure of 5-HT_{2B} was recently determined at a synchrotron (5-HT_{2B-cryo}) (34); thus, the room temperature SFX 5-HT_{2B} structure (5-HT_{2B-RT}) provides the first opportunity to compare membrane protein crystal structures for which data were collected at both ~293 K and ~100 K for these radiation-sensitive crystals (Figure X). While the overall structure of the receptor is quite similar at the two temperatures ($C\alpha$ RMSD < 0.5 Å) some differences were apparent. Because the two 5-HT_{2B} structures were determined at similar resolutions (2.8 Å and 2.7 Å, respectively) and crystal conditions; their side chains could be assigned and B-factors compared with reasonable confidence. For the higher temperature 5-HT_{2B-RT}, and thus greater expected thermal fluctuation, the Wilson B and average B-factors were elevated considerably, 115.7 and 88.4 Å² for 5-HT_{2B-RT} and 72.1 and 67.2 Å² for 5-HT_{2B-RT-cryo}, and most of the significant differences resided in extracellular loop regions. The overall increase in B-factors for 5-HT_{2B-RT} may be attributed to Bragg reflection gating during longer XFEL pulses (12); yet, considering the role these extracellular loops play in substrate binding kinetics (35,36), the significant B-factor discrepancies at these sites may reflect actual temperature-dependent dynamics. Several side chain rotamers in 5-HT_{2B-RT} are rearranged relative to 5-HT_{2B-cryo} (Figure XA), which has been attributed to flash-cooling dependent repacking in soluble protein examples (32). In 5-HT_{2B-cryo}, the extracellular face of helix II forms a water-mediated helical kink at T114, whereas the

absence of this water in 5-HT_{2B-RT} results in a regular helical turn (Figure XB). Furthermore, a few salt bridge pairs are better realized in 5-HT_{2B-RT}, (Figure XC), which may be attributed to the inverse relationship of water's dielectric constant with temperature. Taken together, these differences lead the authors to suggest that the room temperature SFX structure represents a more realistic depiction of the 5-HT_{2B} receptor.

Photosynthetic membrane-embedded proteins have played an essential role in the development of biomolecular imaging with XFELs. Nanocrystallography pioneers chose photosystem I (PS I), a ~1 MDa membrane-embedded multi-protein complex with associated cofactors, as the proof-of-principle sample for SFX (3). The crystal decay of a PS I-ferredoxin complex, as initiated by the electron transfer from PS I to and subsequent dissociation of ferredoxin with a 532 nm green laser, was used as the first demonstration of a pump-probe experimental setup at LCLS (37). These PS I-containing crystals were prepared *in surfo*, a common method for solubilizing membrane proteins.

As discussed previously, membrane proteins may be crystallized *in meso* in lipidic mimetic environments, including LCP. When LCP is combined with swelling agents, such as PEGs or Jeffamine, a lipidic sponge phase (LSP) results, which has approximately the same viscosity as water (38). Crystals of the photosynthetic reaction center from *Blastochloris viridis* (RC_{vir}) have been previously produced in LSP (39), and the relatively small size of this photoactive protein (135 kDa) enabled an elegant time-resolved room temperature Laue diffraction study with synchrotron X-rays that revealed photo-induced structural changes (40). The low viscosity of LSP and a clever scaling-up procedure permitted RC_{vir} microcrystals to be injected via the GVDN and imaged with LCLS X-rays, ultimately resulting in a 3.5-Å dataset, the first high-resolution SFX structure of a membrane protein (41). Despite an estimated 50 times the damage radiation dose for room temperature data collection, a known radiation-sensitive thioether covalent bond between a cysteine and a diacylglycerol molecule (39) was easily

discernible in the electron density, providing a benchmark validation of the “diffract-before-destroy” principle of femtosecond X-ray diffraction for an integral membrane protein.

Insights into dioxygen production from water oxidation, as catalyzed by Photosystem II (PS II) has been of great interest to structural biologists. While conventional crystallography has yielded a recent 1.9-Å structure of the massive membrane protein complex (42), structural insights into the oxygen-evolving complex have been lacking, due to the heavy radiation damage these Mn_4CaO_5 sites absorb during data collection. An SFX report with PS II microcrystals diffracted 9 keV LCLS pulses out to 5.4-Å resolution, yielding a 6.5-Å dataset (17). While a low-resolution result, the transmembrane helices of the photosynthetic reaction center and most of the protein subunits and cofactors were identified in the electron density. Furthermore, the atoms corresponding to the oxygen-evolving complex and non-heme Fe ions were omitted from the initial search model, and significant difference density for these sites was identified.

- PSII Kupitz/Fromme (?) - **Matthias**

Femtosecond X-ray analysis of proteins like PS II is not limited to diffraction alone; indeed, rich electronic and geometrical structural information of redox-active metal complexes may be extracted from X-ray absorption spectroscopy (XAS) and X-ray emission spectroscopy (XES). A recent report demonstrated the feasibility of differentiating 3d transition metal absorption signal at the L-edge from the overwhelming signal of oxygen K-edge, using Mn^{2+} as the test case (43). XES is particularly suitable to SFX experiments, where spectra can be recorded shot-by-shot without scanning the X-ray energy. Using a custom dispersive X-ray spectrometer (44) with hard X-rays at the LCLS, it was shown that $Mn_2^{III,IV}Terpy$, a redox-active model Mn cluster that contains the oxygen-bridging chemistry associated with several metalloenzymes including PS II, does not undergo X-ray induced oxidative damage regardless of photon energy or flux, an important proof-of-concept for measuring emission spectroscopy with XFELs (45). This result permitted a simultaneous X-ray diffraction and XES study of optically pumped ($S_1 \rightarrow S_2$) PS II, which revealed that the microcrystals used in the room-temperature experiment contain

undamaged (Mn^{III} and Mn^{IV}) oxygen-evolving complexes (18). Datasets for the two states were cutoff at 5.7 Å and 5.9 Å for S_1 and S_2 , respectively, and at this resolution, no discernable differences in the electron density were evident, as expected. Furthermore, a higher signal to noise ratio would be required to resolve the expected emission spectral shift between the dark and illuminated states. Regardless, the experiment represents a landmark demonstration of the usefulness of XFELs for structure-function relationships that involve radiation-sensitive biomolecules. Future work on improving microcrystal quality and sample introduction may yield higher resolution information about this important redox center that catalyzes the splitting of water into most of the Earth's molecular oxygen.

Diffraction from Two-dimensional protein crystals

Two-dimensional (2D) crystallography has proven to be a useful and desirable method for the 3D structure determination of membrane protein, as 2D crystals are in principle easier to produce than 3D crystals and represent a near-native environment for membrane proteins arranged on a 2D lipid bilayer (46). Electron microscopy, especially of cryocooled specimens, has been the only tractable method for obtaining Bragg diffraction in transmission from microscopic 2D crystals of nanometer thickness due to the limiting nature of X-ray radiation damage. However, the “diffract-before-destroy” principle of XFELs was recently extended to 2D crystals of soluble streptavidin and the naturally-occurring purple membrane, which consists of 2D sheets of bacteriorhodopsin (bR). In this work, 2D crystals were applied to wafers containing thin layers of Si_4N_3 and imaged at CXI via fixed-target sample delivery strategies, and diffraction images resulting from single 2D crystals were serially recorded out to ~8-Å resolution (45). Careful selection and merging of single diffraction patterns results in an increase in signal-to-noise, which was used to extend this resolution to ~7 Å from 10-15 individual patterns (47) (Figure Y). As opposed to cryoelectron microscopy, these experiments were conducted at room temperature, which paves the way for fast time-resolved diffraction measurements to observe stimulated

structural changes. Much work remains for serial femtosecond 2D crystallography to become a viable alternative and/or complement to electron microscopy, as sample preparations must be tailored to the larger volume required for serial snapshot crystallography, protecting sensitive samples from vacuum, and collection of data from samples tilted in the z-direction for 3D structure reconstruction.

Future directions

The emergence of XFELs does not in any way herald the end of synchrotron and electron radiation sources employed for the structural description of biomolecules at atomic resolution. On the contrary, the emergence of SFX has ushered in sophisticated data collection schemes at a synchrotron using microfocus capabilities under cryocooled conditions from the same CathepsinB microcrystals, resulting in serial synchrotron crystallography (48). Previously, electron diffraction (ED) could only be derived from 2D crystals, but a novel method called microED produced a 3.X-Å resolution structure of HEW lysozyme, collected serially from cryocooled 3D microcrystals (49). Both of these methods carefully selected the radiation dose to maximize crystal rotation and exposure to yield high-quality data. One can clearly see an intriguing synergy emerging between synchrotron, EM, and XFEL sources to give structural biologists a plethora of tools for extracting high-resolution information from tiny crystals, as well as a pipeline or workflow for quality control and experimental design for sophisticated time-resolved measurements that require the room-temperature data collection of XFELs.

- Self-seeding (50) & improvements to the physics?
- Detectors (?)
- NSF center (focus on sample prep)
- Nonperiodic single particles (51) and imaging (52)
- Nanocrystallography -Sample delivery & accessibility (PCS)
- Moving to higher EV and European XFEL

- other anomalous
- Higher rep rates
- Time resolved (?)
- run 9 experiments (?)

Figures

- Experimental setup at CXI/LCLS (liquid/LCP jet/fixed target, pump laser, detectors)
 - Picture of our fixed targets on holder; J.E. *in situ* chips?
 - LCP jet image(s) from U.W.?

Figure X. Structure comparison of human 5-HT_{2B} receptor at cryogenic and room temperatures. In the center is a structural overlay of 5-HT_{2B-RT} (PDB Code: 4NC3 (23) *salmon*) onto 5-HT_{2B-cryo} (PDB Code: 4IB4 (34), *light blue*) using MatchMaker in Chimera (53). Atomic radii for 5-HT_{2B-RT} are based on B-factor differences between the two structures (5-HT_{2B-RT} - 5-HT_{2B-cryo}) where radii range from differences $\leq 21 \text{ \AA}^2$ to $\geq 50 \text{ \AA}^2$. Dotted lines represent predicted lipid bilayer boundaries, as in ref (23). (A) Example of a rotamer difference, Y87, which forms a hydrogen bond with N90 in 5-HT_{2B-RT}. (B) Example of a salt bridge formation between R213 and E196 in 5-HT_{2B-RT}; density beyond the E196 β -carbon was not evident in 5-HT_{2B-cryo}. (C) At the tip of helix II, T114 forms a regular *i*-4 hydrogen bond with I110 in 5-HT_{2B-RT}, while an ordered water occupies this position in 5-HT_{2B-cryo}, stabilizing a helical kink.

Figure Y. Femtosecond X-ray diffraction in transmission from a single bR 2D crystal. The magenta circle corresponds to 10- \AA resolution in reciprocal space. Peaks of resolution $\leq 7 \text{ \AA}$ identified with red circles are of higher intensity used to orient the lattice, while other expected peaks are contained in blue circles. Examples of three-fold symmetrically-related lattice points are labeled black and green, according to the 2D lattice vectors a^* and b^* . Data were collected on a CSPAD detector in the 0.1 μm sample environment of the CXI instrument using LCLS X-rays of 8.8 keV and a nominal pulse energy of $\sim 2 \text{ mJ}$. Image courtesy of Bill Pedrini (47).

- Table: comparing sample delivery methods (similar to supplement in (22) with “theoretical” fixed targets M.S.H.)

	PSI (3)	PSII (17)	5-HT _{2B} (23)	Fixed-target (theoretical)
Crystal medium	Liquid	Liquid	LCP	Liquid-oil emersion
Delivery mechanism	GDVN	electrospin	LCP injector	film on stage
Crystal density	10^{11} (?)		$\sim 5 \times 10^7$ (?)	
Frame rate (Hz)	120	120	120	
Hit rate %	6	5.7	3.6	
Sample consumption (volume and mass)	10 mL 10 mg	0.8 mL 1 mM	0.1 mL 0.3 mg	
Flow rate ($\mu\text{L min}^{-1}$)	10	2.8	0.17	
Consumed protein per 10^4 indexed patterns	6.5 mg		0.091 mg	
Time per 10^4 indexed patterns				

Acknowledgements

This work was supported by LLNL Lab-Directed Research and Development (LDRD) Project 012-ERD-031 (to M.F.), and was performed under the auspices of the U.S. Department of Energy by Lawrence Livermore National Laboratory under contract DE-AC52-07NA27344.

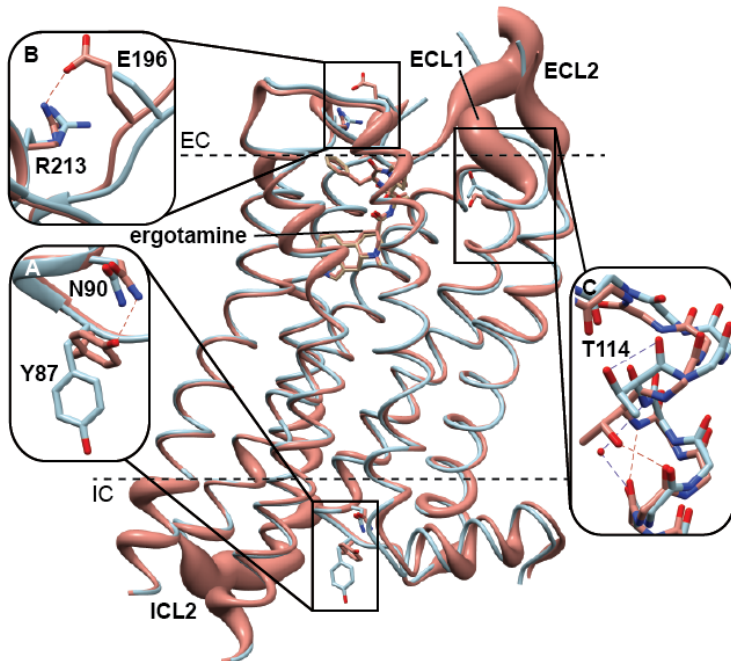


Figure X

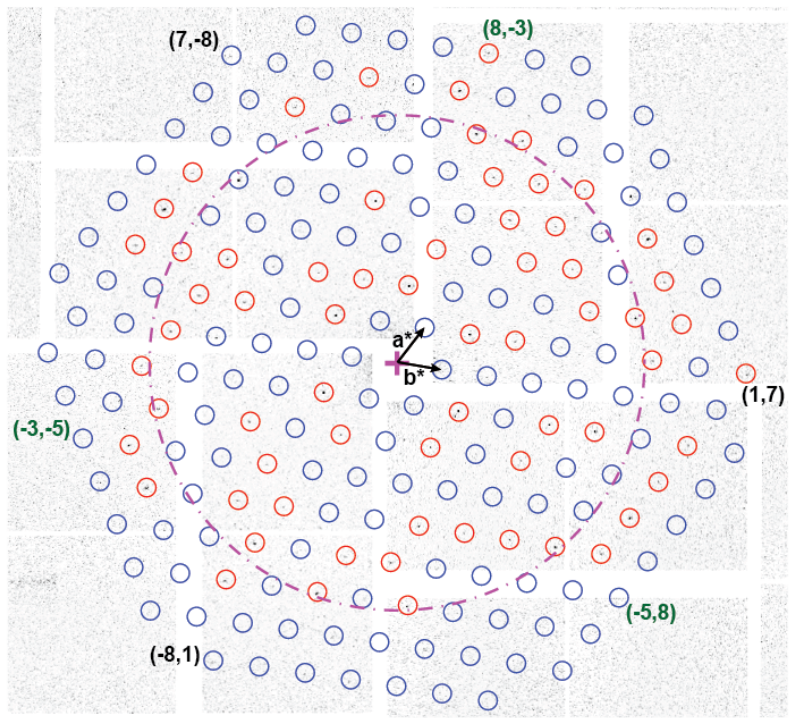


Figure Y

References

1. Neutze, R., Wouts, R., van der Spoel, D., Weckert, E., and Hajdu, J. (2000) Potential for biomolecular imaging with femtosecond X-ray pulses. *Nature* 406, 752-757
2. Waldrop, M. M. (2014) X-ray science: The big guns. *Nature* 505, 604-606
3. Chapman, H. N., Fromme, P., Barty, A., White, T. a., Kirian, R. a., Aquila, A., Hunter, M. S., Schulz, J., DePonte, D. P., Weierstall, U., Doak, R. B., Maia, F. R. N. C., Martin, A. V., Schlichting, I., Lomb, L., Coppola, N., Shoeman, R. L., Epp, S. W., Hartmann, R., Rolles, D., Rudenko, A., Foucar, L., Kimmel, N., Weidenspointner, G., Holl, P., Liang, M., Barthelmess, M., Caleman, C., Boutet, S., Bogan, M. J., Krzywinski, J., Bostedt, C., Bajt, S., Gumprecht, L., Rudek, B., Erk, B., Schmidt, C., Hömke, A., Reich, C., Pietschner, D., Strüder, L., Hauser, G., Gorke, H., Ullrich, J., Herrmann, S., Schaller, G., Schopper, F., Soltau, H., Kühnel, K.-U., Messerschmidt, M., Bozek, J. D., Hau-Riege, S. P., Frank, M., Hampton, C. Y., Sierra, R. G., Starodub, D., Williams, G. J., Hajdu, J., Timneanu, N., Seibert, M. M., Andreasson, J., Rocker, A., Jönsson, O., Svenda, M., Stern, S., Nass, K., Andritschke, R., Schröter, C.-D., Krasniqi, F., Bott, M., Schmidt, K. E., Wang, X., Grotjohann, I., Holton, J. M., Barends, T. R. M., Neutze, R., Marchesini, S., Fromme, R., Schorb, S., Rupp, D., Adolph, M., Gorkhover, T., Andersson, I., Hirsemann, H., Potdevin, G., Graafsma, H., Nilsson, B., and Spence, J. C. H. (2011) Femtosecond X-ray protein nanocrystallography. *Nature* 470, 73-77
4. Boutet, S., Lomb, L., Williams, G. J., Barends, T. R. M., Aquila, A., Doak, R. B., Weierstall, U., DePonte, D. P., Steinbrener, J., Shoeman, R. L., Messerschmidt, M., Barty, A., White, T. A., Kassemeyer, S., Kirian, R. A., Seibert, M. M., Montanez, P. A., Kenney, C., Herbst, R., Hart, P., Pines, J., Haller, G., Gruner, S. M., Philipp, H. T., Tate, M. W., Hromalik, M., Koerner, L. J., van Bakel, N., Morse, J., Ghonsalves, W., Arnlund, D., Bogan, M. J., Caleman, C., Fromme, R., Hampton, C. Y., Hunter, M. S., Johansson, L. C., Katona, G., Kupitz, C., Liang, M., Martin, A. V., Nass, K., Redecke, L., Stellato, F., Timneanu, N., Wang, D., Zatsepin, N. A., Schafer, D., Defever, J., Neutze, R., Fromme, P., Spence, J. C. H., Chapman, H. N., and Schlichting, I. (2012) High-Resolution Protein Structure Determination by Serial Femtosecond Crystallography. *Science* 337, 362-364
5. Seibert, M. M., Ekeberg, T., Maia, F. R., Svenda, M., Andreasson, J., Jonsson, O., Odic, D., Iwan, B., Rocker, A., Westphal, D., Hantke, M., DePonte, D. P., Barty, A., Schulz, J., Gumprecht, L., Coppola, N., Aquila, A., Liang, M., White, T. A., Martin, A., Caleman, C., Stern, S., Abergel, C., Seltzer, V., Claverie, J. M., Bostedt, C., Bozek, J. D., Boutet, S., Miahnahri, A. A., Messerschmidt, M., Krzywinski, J., Williams, G., Hodgson, K. O., Bogan, M. J., Hampton, C. Y., Sierra, R. G., Starodub, D., Andersson, I., Bajt, S., Barthelmess, M., Spence, J. C., Fromme, P., Weierstall, U., Kirian, R., Hunter, M., Doak, R. B., Marchesini, S., Hau-Riege, S. P., Frank, M., Shoeman, R. L., Lomb, L., Epp, S. W., Hartmann, R., Rolles, D., Rudenko, A., Schmidt, C., Foucar, L., Kimmel, N., Holl, P., Rudek, B., Erk, B., Homke, A., Reich, C., Pietschner, D., Weidenspointner, G., Struder, L., Hauser, G., Gorke, H., Ullrich, J., Schlichting, I., Herrmann, S., Schaller, G., Schopper, F., Soltau, H., Kühnel, K. U., Andritschke, R., Schröter, C. D., Krasniqi, F., Bott, M., Schorb, S., Rupp, D., Adolph, M., Gorkhover, T., Hirsemann, H., Potdevin, G., Graafsma, H., Nilsson, B., Chapman, H. N., and Hajdu, J.

- (2011) Single mimivirus particles intercepted and imaged with an X-ray laser. *Nature* 470, 78-81
6. Kimura, T., Joti, Y., Shibuya, A., Song, C., Kim, S., Tono, K., Yabashi, M., Tamakoshi, M., Moriya, T., Oshima, T., Ishikawa, T., Bessho, Y., and Nishino, Y. (2014) Imaging live cell in micro-liquid enclosure by X-ray laser diffraction. *Nature communications* 5, 3052
7. Neutze, R., and Moffat, K. (2012) Time-resolved structural studies at synchrotrons and X-ray free electron lasers: opportunities and challenges. *Current opinion in structural biology* 22, 651-659
8. Boutet, S., and J Williams, G. (2010) The Coherent X-ray Imaging (CXI) instrument at the Linac Coherent Light Source (LCLS). *New Journal of Physics* 12, 035024
9. Spence, J. C. H., Weierstall, U., and Chapman, H. N. (2012) X-ray lasers for structural and dynamic biology. *Reports on progress in physics. Physical Society (Great Britain)* 75, 102601
10. Bogan, M. J. (2013) X-ray Free Electron Lasers Motivate Bioanalytical Characterization of Protein Nanocrystals: Serial Femtosecond Crystallography. *Analytical chemistry* 85, 3464-3471
11. Schlichting, I., and Miao, J. (2012) Emerging opportunities in structural biology with X-ray free-electron lasers. *Current opinion in structural biology* 22, 613-626
12. Barty, A., Caleman, C., Aquila, A., Timneanu, N., Lomb, L., White, T. A., Andreasson, J., Arnlund, D., Bajt, S., Barends, T. R. M., Barthelmess, M., Bogan, M. J., Bostedt, C., Bozek, J. D., Coffee, R., Coppola, N., Davidsson, J., DePonte, D. P., Doak, R. B., Ekeberg, T., Elser, V., Epp, S. W., Erk, B., Fleckenstein, H., Foucar, L., Fromme, P., Graafsma, H., Gumprecht, L., Hajdu, J., Hampton, C. Y., Hartmann, R., Hartmann, A., Hauser, G., Hirsemann, H., Holl, P., Hunter, M. S., Johansson, L., Kassemeyer, S., Kimmel, N., Kirian, R. A., Liang, M., Maia, F. R. N. C., Malmerberg, E., Marchesini, S., Martin, A. V., Nass, K., Neutze, R., Reich, C., Rolles, D., Rudek, B., Rudenko, A., Scott, H., Schlichting, I., Schulz, J., Seibert, M. M., Shoeman, R. L., Sierra, R. G., Soltau, H., Spence, J. C. H., Stellato, F., Stern, S., Strüder, L., Ullrich, J., Wang, X., Weidenspointner, G., Weierstall, U., Wunderer, C. B., and Chapman, H. N. (2011) Self-terminating diffraction gates femtosecond X-ray nanocrystallography measurements. *Nature Photonics* 6, 35-40
13. Lomb, L., Barends, T., Kassemeyer, S., Aquila, A., Epp, S., Erk, B., Foucar, L., Hartmann, R., Rudek, B., Rolles, D., Rudenko, A., Shoeman, R., Andreasson, J., Bajt, S., Barthelmess, M., Barty, A., Bogan, M., Bostedt, C., Bozek, J., Caleman, C., Coffee, R., Coppola, N., DePonte, D., Doak, R. B., Ekeberg, T., Fleckenstein, H., Fromme, P., Gebhardt, M., Graafsma, H., Gumprecht, L., Hampton, C., Hartmann, A., Hauser, G., Hirsemann, H., Holl, P., Holton, J., Hunter, M., Kabsch, W., Kimmel, N., Kirian, R., Liang, M., Maia, F. R. N., Meinhart, A., Marchesini, S., Martin, A., Nass, K., Reich, C., Schulz, J., Seibert, M. M., Sierra, R., Soltau, H., Spence, J. C., Steinbrener, J., Stellato, F., Stern, S., Timneanu, N., Wang, X., Weidenspointner, G., Weierstall, U., White, T., Wunderer, C., Chapman, H., Ullrich, J., Strüder, L., and Schlichting, I. (2011) Radiation damage in protein serial femtosecond crystallography using an x-ray free-electron laser. *Physical Review B* 84, 214111

14. Koopmann, R., Cupelli, K., Redecke, L., Nass, K., DePonte, D. P., White, T. A., Stellato, F., Rehders, D., Liang, M., Andreasson, J., Aquila, A., Bajt, S., Barthelmess, M., Barty, A., Bogan, M. J., Bostedt, C., Boutet, S., Bozek, J. D., Caleman, C., Coppola, N., Davidsson, J., Doak, R. B., Ekeberg, T., Epp, S. W., Erk, B., Fleckenstein, H., Foucar, L., Graafsma, H., Gumprecht, L., Hajdu, J., Hampton, C. Y., Hartmann, A., Hartmann, R., Hauser, G., Hirsemann, H., Holl, P., Hunter, M. S., Kassemeyer, S., Kirian, R. A., Lomb, L., Maia, F. R. N. C., Kimmel, N., Martin, A. V., Messerschmidt, M., Reich, C., Rolles, D., Rudek, B., Rudenko, A., Schlichting, I., Schulz, J., Seibert, M. M., Shoeman, R. L., Sierra, R. G., Soltau, H., Stern, S., Strüder, L., Timneanu, N., Ullrich, J., Wang, X., Weidenspointner, G., Weierstall, U., Williams, G. J., Wunderer, C. B., Fromme, P., Spence, J. C. H., Stehle, T., Chapman, H. N., Betzel, C., and Duszenko, M. (2012) In vivo protein crystallization opens new routes in structural biology. *Nature methods* 9, 259-262
15. Redecke, L., Nass, K., DePonte, D. P., White, T. a., Rehders, D., Barty, a., Stellato, F., Liang, M., Barends, T. R. M., Boutet, S., Williams, G. J., Messerschmidt, M., Seibert, M. M., Aquila, a., Arnlund, D., Bajt, S., Barth, T., Bogan, M. J., Caleman, C., Chao, T.-C., Doak, R. B., Fleckenstein, H., Frank, M., Fromme, R., Galli, L., Grotjohann, I., Hunter, M. S., Johansson, L. C., Kassemeyer, S., Katona, G., Kirian, R. a., Koopmann, R., Kupitz, C., Lomb, L., Martin, a. V., Mogk, S., Neutze, R., Shoeman, R. L., Steinbrener, J., Timneanu, N., Wang, D., Weierstall, U., Zatsepin, N. a., Spence, J. C. H., Fromme, P., Schlichting, I., Duszenko, M., Betzel, C., and Chapman, H. N. (2012) Natively Inhibited Trypanosoma brucei Cathepsin B Structure Determined by Using an X-ray Laser. *Science* 227
16. Weierstall, U., Spence, J. C., and Doak, R. B. (2012) Injector for scattering measurements on fully solvated biospecies. *The Review of scientific instruments* 83, 035108
17. Kern, J., Alonso-Mori, R., Hellmich, J., Tran, R., Hattne, J., Laksmono, H., Glockner, C., Echols, N., Sierra, R. G., Sellberg, J., Lassalle-Kaiser, B., Gildea, R. J., Glatzel, P., Grosse-Kunstleve, R. W., Latimer, M. J., McQueen, T. A., DiFiore, D., Fry, A. R., Messerschmidt, M., Miahnahri, A., Schafer, D. W., Seibert, M. M., Sokaras, D., Weng, T. C., Zwart, P. H., White, W. E., Adams, P. D., Bogan, M. J., Boutet, S., Williams, G. J., Messinger, J., Sauter, N. K., Zouni, A., Bergmann, U., Yano, J., and Yachandra, V. K. (2012) Room temperature femtosecond X-ray diffraction of photosystem II microcrystals. *Porceed Natl Acad Sci U.S.A.*
18. Kern, J., Alonso-Mori, R., Tran, R., Hattne, J., Gildea, R. J., Echols, N., Glöckner, C., Hellmich, J., Laksmono, H., Sierra, R. G., Lassalle-Kaiser, B., Koroidov, S., Lampe, A., Han, G., Gul, S., Difiore, D., Milathianaki, D., Fry, A. R., Miahnahri, A., Schafer, D. W., Messerschmidt, M., Seibert, M. M., Koglin, J. E., Sokaras, D., Weng, T.-C., Sellberg, J., Latimer, M. J., Grosse-Kunstleve, R. W., Zwart, P. H., White, W. E., Glatzel, P., Adams, P. D., Bogan, M. J., Williams, G. J., Boutet, S., Messinger, J., Zouni, A., Sauter, N. K., Yachandra, V. K., Bergmann, U., and Yano, J. (2013) Simultaneous Femtosecond X-ray Spectroscopy and Diffraction of Photosystem II at Room Temperature. *Science*, 1-7
19. Demirci, H., Sierra, R. G., Laksmono, H., Shoeman, R. L., Botha, S., Barends, T. R., Nass, K., Schlichting, I., Doak, R. B., Gati, C., Williams, G. J., Boutet, S., Messerschmidt, M., Jogl, G., Dahlberg, A. E., Gregory, S. T., and Bogan, M. J. (2013) Serial femtosecond X-ray diffraction of 30S ribosomal

- subunit microcrystals in liquid suspension at ambient temperature using an X-ray free-electron laser. *Acta crystallographica. Section F, Structural biology and crystallization communications* 69, 1066-1069
20. Sierra, R. G., Laksmono, H., Kern, J., Tran, R., Hattne, J., Alonso-Mori, R., Lassalle-Kaiser, B., Glockner, C., Hellmich, J., Schafer, D. W., Echols, N., Gildea, R. J., Grosse-Kunstleve, R. W., Sellberg, J., McQueen, T. A., Fry, A. R., Messerschmidt, M. M., Miahnahri, A., Seibert, M. M., Hampton, C. Y., Starodub, D., Loh, N. D., Sokaras, D., Weng, T. C., Zwart, P. H., Glatzel, P., Milathianaki, D., White, W. E., Adams, P. D., Williams, G. J., Boutet, S., Zouni, A., Messinger, J., Sauter, N. K., Bergmann, U., Yano, J., Yachandra, V. K., and Bogan, M. J. (2012) Nanoflow electrospinning serial femtosecond crystallography. *Acta crystallographica. Section D, Biological crystallography* 68, 1584-1587
21. Cherezov, V. (2011) Lipidic cubic phase technologies for membrane protein structural studies. *Current opinion in structural biology* 21, 559-566
22. Weierstall, U., James, D., Wang, C., White, T. A., Wang, D., Liu, W., Spence, J. C., Bruce Doak, R., Nelson, G., Fromme, P., Fromme, R., Grotjohann, I., Kupitz, C., Zatsepин, N. A., Liu, H., Basu, S., Wacker, D., Han, G. W., Katritch, V., Boutet, S., Messerschmidt, M., Williams, G. J., Koglin, J. E., Marvin Seibert, M., Klinker, M., Gati, C., Shoeman, R. L., Barty, A., Chapman, H. N., Kirian, R. A., Beyerlein, K. R., Stevens, R. C., Li, D., Shah, S. T., Howe, N., Caffrey, M., and Cherezov, V. (2014) Lipidic cubic phase injector facilitates membrane protein serial femtosecond crystallography. *Nature communications* 5, 3309
23. Liu, W., Wacker, D., Gati, C., Han, G. W., James, D., Wang, D., Nelson, G., Weierstall, U., Katritch, V., Barty, A., Zatsepин, N. A., Li, D., Messerschmidt, M., Boutet, S., Williams, G. J., Koglin, J. E., Seibert, M. M., Wang, C., Shah, S. T., Basu, S., Fromme, R., Kupitz, C., Rendek, K. N., Grotjohann, I., Fromme, P., Kirian, R. A., Beyerlein, K. R., White, T. A., Chapman, H. N., Caffrey, M., Spence, J. C., Stevens, R. C., and Cherezov, V. (2013) Serial femtosecond crystallography of G protein-coupled receptors. *Science* 342, 1521-1524
24. Zarrine-Afsar, A., Barends, T. R. M., Müller, C., Fuchs, M. R., Lomb, L., Schlichting, I., and Miller, R. J. D. (2012) Crystallography on a chip. *Acta crystallographica. Section D, Biological crystallography* 68, 321-323
25. White, T. A., Barty, A., Stellato, F., Holton, J. M., Kirian, R. A., Zatsepин, N. A., and Chapman, H. N. (2013) Crystallographic data processing for free-electron laser sources. *Acta crystallographica. Section D, Biological crystallography* 69, 1231-1240
26. White, T. A., Kirian, R. A., Martin, A. V., Aquila, A., Nass, K., Barty, A., and Chapman, H. N. (2012) CrystFEL: a software suite for snapshot serial crystallography. *Journal of Applied Crystallography* 45, 335-341
27. Kirian, R. A., Wang, X., Weierstall, U., Schmidt, K. E., Spence, J. C., Hunter, M., Fromme, P., White, T., Chapman, H. N., and Holton, J. (2010) Femtosecond protein nanocrystallography-data analysis methods. *Optics express* 18, 5713-5723
28. Sauter, N. K., Hattne, J., Grosse-Kunstleve, R. W., and Echols, N. (2013) New Python-based methods for data processing. *Acta crystallographica. Section D, Biological crystallography* 69, 1274-1282
29. Hattne, J., Echols, N., Tran, R., Kern, J., Gildea, R. J., Brewster, A. S., Alonso-Mori, R., Glockner, C., Hellmich, J., Laksmono, H., Sierra, R. G.,

- Lassalle-Kaiser, B., Lampe, A., Han, G., Gul, S., Difiore, D., Milathianaki, D., Fry, A. R., Miahnahri, A., White, W. E., Schafer, D. W., Seibert, M. M., Koglin, J. E., Sokaras, D., Weng, T. C., Sellberg, J., Latimer, M. J., Glatzel, P., Zwart, P. H., Grosse-Kunstleve, R. W., Bogan, M. J., Messerschmidt, M., Williams, G. J., Boutet, S., Messinger, J., Zouni, A., Yano, J., Bergmann, U., Yachandra, V. K., Adams, P. D., and Sauter, N. K. (2014) Accurate macromolecular structures using minimal measurements from X-ray free-electron lasers. *Nature methods*
30. Barends, T. R., Foucar, L., Shoeman, R. L., Bari, S., Epp, S. W., Hartmann, R., Hauser, G., Huth, M., Kieser, C., Lomb, L., Motomura, K., Nagaya, K., Schmidt, C., Strecker, R., Anielski, D., Boll, R., Erk, B., Fukuzawa, H., Hartmann, E., Hatsui, T., Holl, P., Inubushi, Y., Ishikawa, T., Kassemeyer, S., Kaiser, C., Koeck, F., Kunishima, N., Kurka, M., Rolles, D., Rudek, B., Rudenko, A., Sato, T., Schroeter, C. D., Soltau, H., Strueder, L., Tanaka, T., Togashi, T., Tono, K., Ullrich, J., Yase, S., Wada, S. I., Yao, M., Yabashi, M., Ueda, K., and Schlichting, I. (2013) Anomalous signal from S atoms in protein crystallographic data from an X-ray free-electron laser. *Acta crystallographica. Section D, Biological crystallography* 69, 838-842
31. Barends, T. R., Foucar, L., Botha, S., Doak, R. B., Shoeman, R. L., Nass, K., Koglin, J. E., Williams, G. J., Boutet, S., Messerschmidt, M., and Schlichting, I. (2013) De novo protein crystal structure determination from X-ray free-electron laser data. *Nature*
32. Fraser, J. S., van den Bedem, H., Samelson, A. J., Lang, P. T., Holton, J. M., Echols, N., and Alber, T. (2011) Accessing protein conformational ensembles using room-temperature X-ray crystallography. *Proceedings of the National Academy of Sciences of the United States of America* 108, 16247-16252
33. Fenwick, R. B., van den Bedem, H., Fraser, J. S., and Wright, P. E. (2014) Integrated description of protein dynamics from room-temperature X-ray crystallography and NMR. *Proceedings of the National Academy of Sciences of the United States of America* 111, E445-454
34. Wacker, D., Wang, C., Katritch, V., Han, G. W., Huang, X. P., Vardy, E., McCorry, J. D., Jiang, Y., Chu, M., Siu, F. Y., Liu, W., Xu, H. E., Cherezov, V., Roth, B. L., and Stevens, R. C. (2013) Structural features for functional selectivity at serotonin receptors. *Science* 340, 615-619
35. Dror, R. O., Pan, A. C., Arlow, D. H., Borhani, D. W., Maragakis, P., Shan, Y., Xu, H., and Shaw, D. E. (2011) Pathway and mechanism of drug binding to G-protein-coupled receptors. *Proceedings of the National Academy of Sciences of the United States of America* 108, 13118-13123
36. Kruse, A. C., Hu, J., Pan, A. C., Arlow, D. H., Rosenbaum, D. M., Rosemond, E., Green, H. F., Liu, T., Chae, P. S., Dror, R. O., Shaw, D. E., Weis, W. I., Wess, J., and Kobilka, B. K. (2012) Structure and dynamics of the M3 muscarinic acetylcholine receptor. *Nature* 482, 552-556
37. Aquila, A., Hunter, M. S., Doak, R. B., Kirian, R. A., Fromme, P., White, T. A., Andreasson, J., Arnlund, D., Bajt, S., Barends, T. R., Barthelmes, M., Bogan, M. J., Bostedt, C., Bottin, H., Bozek, J. D., Caleman, C., Coppola, N., Davidsson, J., DePonte, D. P., Elser, V., Epp, S. W., Erk, B., Fleckenstein, H., Foucar, L., Frank, M., Fromme, R., Graafsma, H., Grotjohann, I., Gumprecht, L., Hajdu, J., Hampton, C. Y., Hartmann, A., Hartmann, R., Hau-Riege, S., Hauser, G., Hirsemann, H., Holl, P., Holton, J. M., Homke, A., Johansson, L., Kimmel, N., Kassemeyer, S., Krasniqi, F., Kuhnel, K. U., Liang, M., Lomb, L.,

- Malmerberg, E., Marchesini, S., Martin, A. V., Maia, F. R., Messerschmidt, M., Nass, K., Reich, C., Neutze, R., Rolles, D., Rudek, B., Rudenko, A., Schlichting, I., Schmidt, C., Schmidt, K. E., Schulz, J., Seibert, M. M., Shoeman, R. L., Sierra, R., Soltau, H., Starodub, D., Stellato, F., Stern, S., Struder, L., Timneanu, N., Ullrich, J., Wang, X., Williams, G. J., Weidenspointner, G., Weierstall, U., Wunderer, C., Barty, A., Spence, J. C., and Chapman, H. N. (2012) Time-resolved protein nanocrystallography using an X-ray free-electron laser. *Optics express* 20, 2706-2716
38. Wadsten, P., Wohri, A. B., Snijder, A., Katona, G., Gardiner, A. T., Cogdell, R. J., Neutze, R., and Engstrom, S. (2006) Lipidic sponge phase crystallization of membrane proteins. *Journal of molecular biology* 364, 44-53
39. Wohri, A. B., Wahlgren, W. Y., Malmerberg, E., Johansson, L. C., Neutze, R., and Katona, G. (2009) Lipidic sponge phase crystal structure of a photosynthetic reaction center reveals lipids on the protein surface. *Biochemistry* 48, 9831-9838
40. Wohri, A. B., Katona, G., Johansson, L. C., Fritz, E., Malmerberg, E., Andersson, M., Vincent, J., Eklund, M., Cammarata, M., Wulff, M., Davidsson, J., Groenhof, G., and Neutze, R. (2010) Light-induced structural changes in a photosynthetic reaction center caught by Laue diffraction. *Science* 328, 630-633
41. Johansson, L. C., Arnlund, D., Katona, G., White, T. A., Barty, A., DePonte, D. P., Shoeman, R. L., Wickstrand, C., Sharma, A., Williams, G. J., Aquila, A., Bogan, M. J., Caleman, C., Davidsson, J., Doak, R. B., Frank, M., Fromme, R., Galli, L., Grotjohann, I., Hunter, M. S., Kassemeyer, S., Kirian, R. A., Kupitz, C., Liang, M., Lomb, L., Malmerberg, E., Martin, A. V., Messerschmidt, M., Nass, K., Redecke, L., Seibert, M. M., Sjohamn, J., Steinbrener, J., Stellato, F., Wang, D., Wahlgren, W. Y., Weierstall, U., Westenhoff, S., Zatsepin, N. A., Boutet, S., Spence, J. C., Schlichting, I., Chapman, H. N., Fromme, P., and Neutze, R. (2013) Structure of a photosynthetic reaction centre determined by serial femtosecond crystallography. *Nature communications* 4, 2911
42. Umena, Y., Kawakami, K., Shen, J. R., and Kamiya, N. (2011) Crystal structure of oxygen-evolving photosystem II at a resolution of 1.9 Å. *Nature* 473, 55-60
43. Mitzner, R., Rehanek, J., Kern, J., Gul, S., Hattne, J., Taguchi, T., Alonso-Mori, R., Tran, R., Weniger, C., Schroder, H., Quevedo, W., Laksmono, H., Sierra, R. G., Han, G., Lassalle-Kaiser, B., Koroidov, S., Kubicek, K., Schreck, S., Kunnus, K., Brzhezinskaya, M., Firsov, A., Minitti, M. P., Turner, J. J., Moeller, S., Sauter, N. K., Bogan, M. J., Nordlund, D., Schlotter, W. F., Messinger, J., Borovik, A., Techert, S., de Groot, F. M., Fohlisch, A., Erko, A., Bergmann, U., Yachandra, V. K., Wernet, P., and Yano, J. (2013) L-Edge X-ray Absorption Spectroscopy of Dilute Systems Relevant to Metalloproteins Using an X-ray Free-Electron Laser. *The journal of physical chemistry letters* 4, 3641-3647
44. Alonso-Mori, R., Kern, J., Sokaras, D., Weng, T. C., Nordlund, D., Tran, R., Montanez, P., Delor, J., Yachandra, V. K., Yano, J., and Bergmann, U. (2012) A multi-crystal wavelength dispersive x-ray spectrometer. *The Review of scientific instruments* 83, 073114
45. Alonso-Mori, R., Kern, J., Gildea, R. J., Sokaras, D., Weng, T.-C., Lassalle-Kaiser, B., Tran, R., Hattne, J., Laksmono, H., Hellmich, J., Glöckner, C.,

- Echols, N., Sierra, R. G., Schafer, D. W., Sellberg, J., Kenney, C., Herbst, R., Pines, J., Hart, P., Herrmann, S., Grosse-Kunstleve, R. W., Latimer, M. J., Fry, A. R., Messerschmidt, M. M., Miahnahri, A., Seibert, M. M., Zwart, P. H., White, W. E., Adams, P. D., Bogan, M. J., Boutet, S., Williams, G. J., Zouni, A., Messinger, J., Glatzel, P., Sauter, N. K., Yachandra, V. K., Yano, J., and Bergmann, U. (2012) Energy-dispersive X-ray emission spectroscopy using an X-ray free-electron laser in a shot-by-shot mode. *Proc Natl Acad Sci U.S.A.* 109
46. Ubarretxena-Belandia, I., and Stokes, D. L. (2012) Membrane protein structure determination by electron crystallography. *Current opinion in structural biology* 22, 520-528
47. Pedrini, B., Tsai, C.-J., Capitani, G., Padeste, C., Hunter, M. S., Zatsepin, N. A., Barty, A., Benner, W. H., Boutet, S., Feld, G. K., Hau-Riege, S. P., Kirian, R. A., Kupitz, C., Messerschmidt, M., Ogren, J. I., Pardini, T., Segelke, B., Williams, G. J., Spence, J. C. H., Abela, R., Coleman, M., Evans, J. E., Schertler, G., Frank, M., and Li, X.-D. (2014) 7 Å resolution in protein 2D-crystal X-ray diffraction at LCLS. *Phil Trans B* in press
48. Gati, C., Bourenkov, G., Klinge, M., Rehders, D., Stellato, F., Oberthür, D., Yefanov, O., Sommer, B. P., Mogk, S., Duszenko, M., Betzel, C., Schneider, T. R., Chapman, H. N., and Redecke, L. (2014) Serial crystallography on in vivo grown microcrystals using synchrotron radiation. *IUCrJ* 1, 87-94
49. Shi, D., Nannenga, B. L., Iadanza, M. G., and Gonen, T. (2013) Three-dimensional electron crystallography of protein microcrystals. *eLife* 2, e01345
50. Amann, J., Berg, W., Blank, V., and Decker, F. (2012) Demonstration of self-seeding in a hard-X-ray free-electron laser. *Nature Photonics* 6
51. Loh, N. D., Hampton, C. Y., Martin, A. V., Starodub, D., Sierra, R. G., Barty, A., Aquila, A., Schulz, J., Lomb, L., Steinbrener, J., Shoeman, R. L., Kassemeyer, S., Bostedt, C., Bozek, J., Epp, S. W., Erk, B., Hartmann, R., Rolles, D., Rudenko, A., Rudek, B., Foucar, L., Kimmel, N., Weidenspointner, G., Hauser, G., Holl, P., Pedersoli, E., Liang, M., Hunter, M. M., Gumprecht, L., Coppola, N., Wunderer, C., Graafsmo, H., Maia, F. R., N. C., Ekeberg, T., Hantke, M., Fleckenstein, H., Hirsemann, H., Nass, K., White, T. A., Tobias, H. J., Farquar, G. R., Benner, W. H., Hau-Riege, S. P., Reich, C., Hartmann, A., Soltau, H., Marchesini, S., Bajt, S., Barthelmess, M., Bucksbaum, P., Hodgson, K. O., Strüder, L., Ullrich, J., Frank, M., Schlichting, I., Chapman, H. N., and Bogan, M. J. (2012) Fractal morphology, imaging and mass spectrometry of single aerosol particles in flight. *Nature* 486, 513-517
52. Starodub, D., Aquila, A., Bajt, S., Barthelmess, M., Barty, A., Bostedt, C., Bozek, J. D., Coppola, N., Doak, R. B., Epp, S. W., Erk, B., Foucar, L., Gumprecht, L., Hampton, C. Y., Hartmann, A., Hartmann, R., Holl, P., Kassemeyer, S., Kimmel, N., Laksmono, H., Liang, M., Loh, N. D., Lomb, L., Martin, A. V., Nass, K., Reich, C., Rolles, D., Rudek, B., Rudenko, A., Schulz, J., Shoeman, R. L., Sierra, R. G., Soltau, H., Steinbrener, J., Stellato, F., Stern, S., Weidenspointner, G., Frank, M., Ullrich, J., Strüder, L., Schlichting, I., Chapman, H. N., Spence, J. C., and Bogan, M. J. (2012) Single-particle structure determination by correlations of snapshot X-ray diffraction patterns. *Nature communications* 3, 1276
53. Pettersen, E. F., Goddard, T. D., Huang, C. C., Couch, G. S., Greenblatt, D. M., Meng, E. C., and Ferrin, T. E. (2004) UCSF Chimera--a visualization

system for exploratory research and analysis. *Journal of computational chemistry* 25, 1605-1612